JOURNAL OF COMPUTATIONAL PHYSICS 117, 102–113 (1995)

Nonreflecting Boundary Conditions Based on Kirchhoff-Type Formulae

DAN GIVOLI

Department of Aerospace Engineering, Technion—Israel Institute of Technology, Haifa 32000, Israel

AND

DAN COHEN*

Department of Computer Science, Hebrew University, Jerusalem 91904, Israel

Received March 14, 1994

Exact nonreflecting boundary conditions are considered for exterior three-dimensional time-dependent wave problems. These include a nonlocal condition for acoustic waves based on Kirchhoff's formula, orginally proposed by L. Ting and M. J. Miksis (*J. Acoust. Soc. Am.* **80**, 1825 (1986), and an analogous condition for elastic waves. These conditions are computationally attractive in that their temporal nonlocality is limited to a fixed amount of past information. However, when a standard nondissipative finite difference stencil is used as the interior scheme, a long-time instability is exhibited in the numerical solution. This instability is analyzed for a simple one-dimensional model problem. It is eliminated once the standard interior scheme is replaced by the dissipative Lax–Wendroff scheme. In this case stability is demonstrated experimentally, and it is also established theoretically in the one-dimensional case.

INTRODUCTION

The numerical solution of exterior wave problems has caught much attention in the last few years. Such problems occur in many fields of application, including underwater acoustics, geophysics, and electromagnetism. Various numerical methods for the solution of wave problems in infinite domains are discussed in a recent monograph [1]. An important and common method in this category is based on the use of artificial boundaries and nonreflecting boundary conditions. In this paper we concentrate on the use of this method in the context of three-dimensional acoustic and elastic wave problems.

Consider a wave problem in the unbounded domain exterior to a scatterer or an obstacle with boundary Γ, as illustrated in Fig. 1. This problem is to be solved numerically using a finite difference or a finite element method. Since such methods require a *finite* computational domain, the original infinite domain is truncated by introducing an artificial boundary $\mathcal{B}$ around the obstacle. Thus a finite computational domain Ω is defined, which is bounded internally by Γ and externally by $\mathcal{B}$. The infinite domain exterior to $\mathcal{B}$ (namely the domain outside Ω) is denoted D. The position of the artificial boundary $\mathcal{B}$ is chosen such that it encloses all the "irregularities" in the problem domain. Thus in Ω the medium may be inhomogeneous, anisotropic, or even behave nonlinearly, and it may include wave sources and nonzero initial conditions. All these "irregularities" are taken care of by the numerical scheme to be employed in Ω (assuming that it has the appropriate capabilities). On the other hand, in D the medium is usually assumed to be homogeneous, isotropic, and linear, not to include any wave sources, and to be at rest for times $t \leq 0$.

Now, to complete the statement of the problem in Ω, a boundary condition must be imposed on $\mathcal{B}$. This boundary condition should have the property that waves impinging $\mathcal{B}$ from inside Ω are "absorbed" by $\mathcal{B}$ without generating reflection. It is well known that when over-simplified boundary conditions are used on $\mathcal{B}$, they may produce large spurious reflection of waves from $\mathcal{B}$ back into Ω, and thus they may pollute the computed solution. Various special boundary conditions on $\mathcal{B}$ have been proposed by many authors in the last two decades to reduce the amount of spurious reflection or totally annihilate it. These are called non-reflecting boundary conditions (NRBCs). See [2] for a review on the subject. After a NRBC is imposed on $\mathcal{B}$, the statement of the problem in Ω is complete, and a finite difference or a finite element scheme is used in Ω to solve the problem. Of course, the NRBC on $\mathcal{B}$ must be discretized along with the governing field equations in Ω.

NRBCs may be *local* or *nonlocal*. Sequences of local NRBCs with increasing order were proposed, e.g., by Engquist and Majda [3] and Bayliss and Turkel [4], for both the time-dependent and the time-harmonic cases. These NRBCs are approxi-

* Current address: Tecnomatics Technologies Ltd., Delta House, Hertzeliya 46733, Israel.

0021-9991/95 $6.00

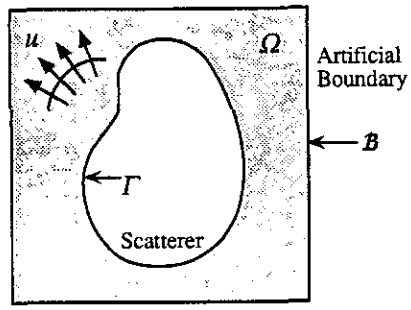

FIG. 1. A typical setup for solving a wave problem in the unbounded domain exterior to a scatterer with boundary Γ. $\mathcal{B}$ is the artifical boundary and Ω is the computational domain. On $\mathcal{B}$, a nonreflecting boundary condition (NRBC) is applied.

mate, and they are local in both space and time. Hagstrom and Keller [5] and Keller and Givoli [6–8] each devised an exact nonlocal NRBC for elliptic problems. The latter NRBC is based on the Dirichlet-to-Neumann map of the differential operator. From a computational standpoint the spatial nonlocality of the NRBC may sometimes be regarded as inconvenient [1], but this is the price one has to pay in order to eliminate the infinite domain D in an *exact* fashion. It turns out [1] that in many cases this price is reasonably small, considering the robustness of the exact NRBC and the high accuracy of the results obtained by using it.

Similarly, in time-dependent problems an *exact* NRBC must be *nonlocal in both space and time,* except in very simple cases. NRBCs which are nonlocal in time were proposed, e.g., in [9–12]. As opposed to the spatial nonlocality of the NRBC, the temporal nonlocality may pose very serious computational difficulties. The main difficulty is related to the fact that the scheme must possess "memory," and thus typically the entire history of the nodal values of the solution on the boundary $\mathcal{B}$ must be accumulated and stored during the solution process. This means that the required computer storage and computing time are ever increasing as time goes on. In two and three dimensions this may render the solution procedure impractical. A simple, although sometimes effective, way to reduce the amount of storage and computational effort is to use a "limited memory" time-stepping technique. In this technique only the data from a limited number of previous time steps are maintained in each time-step, whereas earlier data are deleted and are not used in the computation. The temporally nonlocal NRBCs proposed in [9, 10] employ this procedure.

Another difficulty related to the use of a NRBC which is nonlocal in time is that it may require, on the discrete level, the use of non-standard time-integration schemes for integro-differential systems of equations. This occurs if convolution-type integrals appear in the formulation, as in the case where the Dirichlet-to-Neumann boundary condition [6] is generalized to the time-dependent case in a straightforward manner [1].

The difficulties associated with the nonlocality in time have led most authors to consider only temporally local NRBCs. This was also the thrust for introducing a semidiscrete Dirichlet-to-Neumann NRBC [13] which is spatially nonlocal but temporally local. The latter NRBC, although quite effective, cannot be exact with respect to the original infinite domain problem due to its locality in time.

In this paper we discuss the use of NRBCs which are based on Kirchhoff-type formulae. The idea to use the Kirchhoff formula as a NRBC is originally due to Ting and Miksis, who considered three-dimensional time-dependent acoustic wave problems [14]. This NRBC is *exact* and, thus, unavoidably nonlocal in both space and time, but it does not involve constantly increasing storage space and computing time, since it depends on a *fixed* amount of past information. Moreover, it does not include any convolution integrals. Therefore it avoids the difficulties otherwise associated with nonlocality in time.

In the next section we discuss the Kirchhoff NRBC for three-dimensional acoustic waves. We also derive an analogous condition for three-dimensional elastic waves. In the section that follows we combine the Kirchhoff NRBC with a standard nondissipative finite difference stencil used in the interior of the computational domain Ω. We present the results of some numerical experiments performed in a spherically symmetric case. These results indicate the presence of long-time instabilities in the numerical solution, generated by the Kirchhoff NRBC. We characterize these instabilities and analyze them by considering a simple one-dimensional model problem.

Then we replace the standard interior scheme by the dissipative Lax–Wendroff scheme, and we repeat the numerical experiments in the spherically symmetric case. This time the numerical scheme does not exhibit any instability. We again consider the one-dimensional model problem and show that stability is guaranteed by applying the Goldberg–Tadmor theory. We close the paper with some concluding remarks.

KIRCHHOFF-TYPE NRBC'S

We first consider acoustic waves in the three-dimensional infinite domain $\mathcal{R}$ exterior to an obstacle or a scatterer. The wave $u(\mathbf{x}, t)$ satisfies the scalar wave equation,

$$\frac{\partial^2 u}{\partial t^2} = c^2 \nabla^2 u + f(\mathbf{x}, t), \tag{1}$$

in $\mathcal{R}$. Here t is time, c is the wave speed, and f is a given source function. Some boundary condition is given on the obstacle surface Γ, say the Dirichlet condition,

$$u = g \quad \text{on } \Gamma. \tag{2}$$

Here g is a given function of $\mathbf{x} \in \Gamma$ and time. At time $t = 0$, the initial conditions are given throughout the domain:

$$u(\mathbf{x}, 0) = u_0(\mathbf{x}); \quad \frac{\partial u}{\partial t}(\mathbf{x}, 0) = v_0(\mathbf{x}). \tag{3}$$

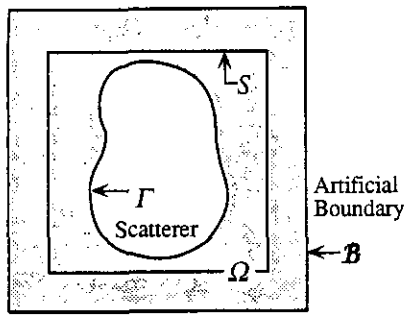

FIG. 2. The setup for using the Kirchhoff-type NRBC. Two artificial boundaries, $\mathcal{S}$ and $\mathcal{B}$, are introduced. The computational domain is bounded internally by Γ and externally by $\mathcal{B}$.

Here u_0 and v_0 are given functions. We assume that the functions f, u_0, and v_0 have finite support. Typically their support is a certain region around the scatterer.

Following Ting and Miksis [14], we now introduce *two* artifical boundaries. The setup is shown in Fig. 2. First, an artificial boundary $\mathcal{S}$ is chosen to enclose the scatterer. Then, some distance away from $\mathcal{S}$, a second artificial boundary $\mathcal{B}$ is introduced. The computational domain Ω is bounded internally by the surface of the scatterer Γ, and externally by $\mathcal{B}$. The boundary $\mathcal{S}$ is chosen to lie outside of the support of f, u_0, and v_0. Thus, outside $\mathcal{S}$ (and, in particular, between $\mathcal{S}$ and $\mathcal{B}$) the homogeneous counterparts of (1) and (3) hold. The choice for the position of $\mathcal{B}$ will be discussed later; however, it is clear that in order to make the computational domain Ω small, $\mathcal{B}$ should be set close to $\mathcal{S}$.

We remark that in the region which lies between Γ and $\mathcal{S}$, a wave equation which is more complicated than (1) may be considered without affecting the validity of the ideas that follow. In particular, the medium in this region may be inhomogeneous or anisotropic, or may behave nonlinearly. A nonlinear behavior in the region around Γ occurs, for example, if the scatterer is covered with a cloud of bubbles.

Next we recall the Kirchhoff formula associated with the wave equation (1). This formula is discussed and proved in [15, 16]; it is a way to express Huygen's principle in three dimensions. Let $\tilde{\mathcal{S}}$ be any closed surface in $\mathcal{R}$ which encloses the scatterer. For example, $\tilde{\mathcal{S}}$ may be Γ or $\mathcal{S}$ or $\mathcal{B}$ in Fig. 2. Denote the infinite domain exterior to $\tilde{\mathcal{S}}$ by $\tilde{\mathcal{R}}$. Let $\mathbf{x}$ be any point in $\tilde{\mathcal{R}}$. Then Kirchhoff's formula is

$$u(\mathbf{x},t) = \frac{1}{4\pi}\int_{\tilde{\mathcal{R}}} \frac{1}{r}[f]\,d\boldsymbol{\xi} - \frac{1}{4\pi}\int_{\tilde{\mathcal{S}}}\left([u]\frac{\partial}{\partial \nu}\left(\frac{1}{r}\right) - \frac{1}{r}\left[\frac{\partial u}{\partial \nu}\right] - \frac{1}{rc}\frac{\partial r}{\partial \nu}\left[\frac{\partial u}{\partial t}\right]\right)d\boldsymbol{\xi}. \tag{4}$$

Here $r = |\mathbf{x} - \boldsymbol{\xi}|$, and $\partial/\partial\nu$ is the normal derivative at $\boldsymbol{\xi}$ on $\tilde{\mathcal{S}}$. The operator $[\cdot]$ is the *retarded value* operator, defined by

$$[f] = f(\boldsymbol{\xi}, \tau)|_{\tau = t - r/c}. \tag{5}$$

Now we return to the setup shown in Fig. 2. We choose $\tilde{\mathcal{S}} = \mathcal{S}$, and we choose $\mathbf{x}$ to lie on the boundary $\mathcal{B}$. Now since $f \equiv 0$ in the domain exterior to $\mathcal{S}$, the first term in (4) drops out, and we are left with

$$u(\mathbf{x},t) = -\frac{1}{4\pi}\int_{\mathcal{S}}\left([u]\frac{\partial}{\partial \nu}\left(\frac{1}{r}\right) - \frac{1}{r}\left[\frac{\partial u}{\partial \nu}\right] - \frac{1}{rc}\frac{\partial r}{\partial \nu}\left[\frac{\partial u}{\partial t}\right]\right)d\boldsymbol{\xi}; \quad \mathbf{x} \in \mathcal{B}. \tag{6}$$

This equation can be used as an exact boundary condition, which involves u on $\mathcal{B}$ and the retarded values of u, $\partial u/\partial \nu$, and $\partial u/\partial t$ on $\mathcal{S}$. The idea to use the Kirchhoff formula as a NRBC is due to Ting and Miksis [14]. However, they did not attempt to implement a numerical scheme that incorporates (6) and to test the actual performance of this NRBC. We shall do this in the next sections.

The exact NRBC (6) is nonlocal in space and time. The nonlocality in time is, however, limited to a fixed amount of past data, because the retarded value $\tau = t - r/c$ is bounded from above and from below, i.e., $t - r_{\max}/c \le \tau \le t - r_{\min}/c$. Here $r_{\min}$ and $r_{\max}$ are the extremal values of r, which are the minimal and maximal distances between the two artificial boundaries, $\mathcal{S}$ and $\mathcal{B}$. For example, if $\mathcal{S}$ and $\mathcal{B}$ are concentric spheres with radii $R_{\mathcal{S}}$ and $R_{\mathcal{B}}$, respectively, then the retarded time τ is in the interval $(R_{\mathcal{B}} - R_{\mathcal{S}})/c \le \tau \le (R_{\mathcal{B}} + R_{\mathcal{S}})/c$. In other words, the memory required by the numerical scheme does not grow in time. Clearly, this is a big advantage of the scheme.

It is interesting to note that the NRBC (6) is inherently three-dimensional. In a sense, the two-dimensional case is harder, because an exact boundary condition in that case would not have a limited nonlocality in time such as in (6). This is related to the fact that the Green's function in even dimensions has an infinitely long "tail."

Now we turn to the case of *elastic waves*. Problems in unbounded domains involving the propagation of elastic waves are typical to geophysics. In this case, the scalar wave equation (1) is replaced by the equations of three-dimensional elastodynamics in the displacement vector field $\mathbf{u}$:

$$m\frac{\partial^2 u_i}{\partial t^2} = \sigma_{ij,j} + f_i, \tag{7}$$

$$\sigma_{ij} = c_{ijkl}u_{k,l}. \tag{8}$$

Here u_i is the displacement component in the i direction ($i = 1, 2, 3$), m is the mass density, σ_{ij} is the stress component, the

c_{ijkl} are the elastic moduli, and f_i is the body force component in the i direction. A comma indicates partial differentiation, and the summation convention with respect to repeated indices is in force. Some boundary conditions are prescribed on the scatterer surface Γ. The initial conditions

$$u_i(\mathbf{x}, 0) = u_{i0}(\mathbf{x}); \quad \frac{\partial u_i}{\partial t}(\mathbf{x}, 0) = v_{i0}(\mathbf{x}), \tag{9}$$

are given throughout the infinite domain $\mathcal{S}$. The setup is again as in Fig. 2. As in the acoustic case, we assume that f_i, u_{i0}, and v_{i0} vanish identically in the domain exterior to $\mathcal{S}$. We also assume that in this domain the medium is homogeneous and isotropic.

We consider the fundamental solution of elastodynamics for a time-dependent concentrated body force which is suddenly applied at time $t = 0$ at a point in an unbounded isotropic three-dimensional medium. See Wheeler and Sternberg [17] and Achenbach [18]. We denote the fundamental solutions for the displacement and stress components, respectively, by

$$u_i^*(\mathbf{x}, t; \boldsymbol{\xi}, k, F(t)), \quad \sigma_{ij}^*(\mathbf{x}, t; \boldsymbol{\xi}, k, F(t)). \tag{10}$$

Here, u_i^* is the displacement component in the i direction at point $\mathbf{x}$ at time t due to a concentrated body force acting at point $\boldsymbol{\xi}$ in the k direction and having the intensity $F(t)$ for $t \geq 0$. The stress σ_{ij}^* has a similar interpretation. These fundamental solutions involve the retarded values of $F(t)$; more specifically they have the forms

$$u_i^* = A_1 \int_{1/c_L}^{1/c_T} sF(t - rs)\,ds + A_2[F]_L + A_3[F]_T, \tag{11}$$

$$\sigma_{ij}^* = B_1 \int_{1/c_L}^{1/c_T} sF(t - rs)\,ds + B_2[F]_L + B_3[F]_T + B_4\left[\frac{\partial F}{\partial t}\right]_L + B_5\left[\frac{\partial F}{\partial t}\right]_T. \tag{12}$$

Here c_L and c_T are the longitudinal and transverse wave speeds, respectively, $r = |\mathbf{x} - \boldsymbol{\xi}|$, and

$$[F]_L = F\left(t - \frac{r}{c_L}\right), \quad [F]_T = F\left(t - \frac{r}{c_T}\right). \tag{13}$$

The coefficients A_i in (11) and B_i in (12) are rational functions involving r as well as the components $x_i - \xi_i$. Their expressions can be found in [17, p. 80]; [18, p. 100].

Now, the following identity can be proved [18, p. 103]:

$$u_k(\mathbf{x}, t) = \frac{1}{4\pi m} \sum_{i=1}^{3} \int_{\mathcal{S}} \{u_i^*(\boldsymbol{\xi}, t; \mathbf{x}, k, n_j \sigma_{ij}(\boldsymbol{\xi}, t)) - n_j \sigma_{ij}^*(\boldsymbol{\xi}, t; \mathbf{x}, k, u_i(\boldsymbol{\xi}, t))\}\,d\boldsymbol{\xi}. \tag{14}$$

Here $\boldsymbol{\xi}$ is a point on $\mathcal{S}$, $\mathbf{x}$ is a point in the domain exterior to $\mathcal{S}$, and n_j is the j component of the unit outward normal to $\mathcal{S}$. Equation (14) is analogous to Kirchhoff's formula in the elastic case. As in the acoustic case, we now choose $\mathbf{x}$ to lie on the boundary $\mathcal{B}$ (see Fig. 2). Then (14) can be used as an exact NRBC, which involves u_k on $\mathcal{B}$ and (via (11)–(13)) the retarded values of u_i, σ_{ij}, and $\partial u_i/\partial t$ on $\mathcal{S}$. As before, this NRBC is nonlocal in space and time, but the nonlocality in time is limited to a fixed amount of past information, depending on the minimal and maximal distances, $r_{\min}$ and $r_{\max}$, between the boundaries $\mathcal{S}$ and $\mathcal{B}$. More specifically, the retarded value $\tau = t - r/c$, involved in the integrand of (14), is bounded from above and from below, i.e., $t - r_{\max}/c_T \leq \tau \leq t - r_{\min}/c_L$ (recall that always $c_T < c_L$).

THE NUMERICAL SCHEME

In this section we consider the case of three-dimensional acoustic waves. We describe in general terms the numerical scheme which is used in the computational domain Ω, incorporating the Kirchhoff NRBC (6).

We choose to employ an *explicit* finite difference stencil for (1) in Ω. This choice is suggested by the fact that (6) is itself an explicit formula, since the value $u(\mathbf{x}, t)$ on the left side of (6) depends only on values at *retarded* times, namely at times not later than $\tau = t - r_{\min}/c$. Therefore, it is natural to combine the explicit formula (6) on $\mathcal{B}$ with an explicit finite difference stencil in Ω, in order to obtain a method which is totally explicit. We use a constant time-step interval Δt and denote the time after n time steps by $t_n = n\Delta t$. We also denote u_A^n the approximate value of the solution u at grid point A at time t_n.

For an interior grid point A, we use some explicit s-level finite difference stencil, of the general form

$$u_A^{n+1} = D_A[\mathbf{u}^n, \mathbf{u}^{n-1}, \ldots, \mathbf{u}^{n-(s-2)}]. \tag{15}$$

Here D_A is an operator, and $\mathbf{u}^n$ is the vector whose entries are the values u_A^n. A specific choice for stencil (15) in the spherically symmetric case will be given in the next section. For a grid point A on the boundary Γ we simply have

$$u_A^{n+1} = g_A^{n+1}, \tag{16}$$

where g_A^{n+1} is the value of the function g (see (2)) at grid point A at time t_{n+1}. Finally, we must obtain a formula which is the discrete version of the Kirchhoff NRBC (6). To this end we first introduce the following approximations that will be used in evaluating the Kirchhoff integral.

1. *Numerical integration,*

$$\int_{\mathcal{S}} f(\boldsymbol{\xi})\,d\boldsymbol{\xi} \simeq \sum_{A \in \eta_{\mathcal{S}}} W_A f_A. \tag{17}$$

here the W_A are constant weights, f_A is the value of f at grid point A, and $\eta_{\mathcal{S}}$ is the set of all grid points on the boundary $\mathcal{S}$.

2. *Linear interpolation between time steps.* If $t \in [t_n, t_{n+1}]$ then we define

$$\hat{f}(t) \equiv \frac{f^{n+1} - f^n}{\Delta t}(t - t_n) + f^n. \tag{18}$$

The function $\hat{f}(t)$ is a continuous piecewise-linear function which interpolates the values f_A at the grid points.

3. *Approximate time and space derivatives,*

$$\frac{\partial}{\partial t} \simeq D_t, \quad \frac{\partial}{\partial \nu} \simeq D_\nu. \tag{19}$$

Here D_t is a difference operator in time, and D_ν is a difference operator in the spatial direction normal to $\mathcal{S}$.

For the time being, we leave the approximations (17) and (19) general; they will be specialized in the next section. Using (17)–(19) in (6), we obtain the discrete version of the NRBC, for a grid point A on the boundary $\mathcal{B}$,

$$u_A^{n+1} = -\frac{1}{4\pi} \sum_{B \in \eta_{\mathcal{S}}} W_B \left([u_B] \frac{\partial}{\partial \nu}\left(\frac{1}{r}\right) - \frac{1}{r}[D_\nu u_B] - \frac{1}{rc}\frac{\partial r}{\partial \nu}[D_t u_B] \right). \tag{20}$$

Here r is the distance between grid points A (on $\mathcal{B}$) and B (on $\mathcal{S}$). The retarded value operator $[\cdot]$ is defined similarly to (5), i.e.,

$$[f_B] = \hat{f}_B(\tau)\big|_{\tau = t_{n+1} - r/c}. \tag{21}$$

This completes the general description of the numerical scheme. It starts from the given initial values u_A^0 of all the grid points, and then steps in time via the formulae (16) for grid points on Γ, (15) for interior grid points, and (20) for grid points on $\mathcal{B}$.

After the solution in the computational domain Ω and on $\mathcal{B}$ is found, we may, in principle, use a discrete version of (4) to obtain an approximate solution in D, namely *outside* of the computational domain. In doing so we choose $\tilde{\mathcal{S}} = \mathcal{B}$, and the first term in (4) drops out as before. However, this requires storing the history of the solution at grid points on $\mathcal{B}$, which we would normally wish to avoid.

NUMERICAL EXPERIMENTS AND LONG-TIME INSTABILITY

We now specialize the numerical procedure in the previous section to the *spherically symmetric* case. The problem considered is governed by Eqs. (1)–(3), and the setup is as in Fig. 2, but Γ, $\mathcal{S}$, and $\mathcal{B}$ are all spherical surfaces, $g(t)$ in (2) is a function of time alone, and we also choose for simplicity $f \equiv 0$ and $u_0 = v_0 \equiv 0$. We refer to a spherical system of coordinates where the radial coordinate is denoted ρ. The radii of Γ, $\mathcal{S}$, and $\mathcal{B}$ are denoted $R_\Gamma, R_{\mathcal{S}}$, and $R_{\mathcal{B}}$, respectively. We introduce the new variable $v(\rho, t) = \rho u(\rho, t)$, and for convenience, we regard v rather than u as the primal variable. The wave equation (1) reduces in the present case to

$$\frac{\partial^2 v}{\partial t^2} = c^2 \frac{\partial^2 v}{\partial \rho^2}. \tag{22}$$

The boundary condition on Γ is $u = g$ (see (2)), namely $v = R_\Gamma g$. The exact solution of the problem is

$$v(\rho, t) = \begin{cases} 0, & t < (\rho - R_\Gamma)/c \\ R_\Gamma g(t - (\rho - R_\Gamma)/c), & t \geq (\rho - R_\Gamma)/c \end{cases}. \tag{23}$$

Moreover, in the spherically symmetric case (but not in the general case) it is possible to find an exact NRBC on $\mathcal{B}$ which is purely *local* [1]. This NRBC is

$$c\frac{\partial v}{\partial \rho} + \frac{\partial v}{\partial t} = 0 \quad \text{on } \mathcal{B}. \tag{24}$$

We shall compare the numerical solution obtained using the nonlocal Kirchhoff NRBC (6) with that obtained by using the local NRBC (24) on $\mathcal{B}$ and with the exact solution (23).

In the computational domain Ω we use equally spaced grid points in the radial direction and denote the spacing h. The interior stencil (15) is chosen to be the standard non-dissipative central difference stencil for the wave equation, namely,

$$v_A^{n+1} = \left(\frac{c\Delta t}{h}\right)^2 (v_{A+1}^n - 2v_A^n + v_{A-1}^n) + 2v_A^n - v_A^{n-1}. \tag{25}$$

This stencil is known to be stable if the Courant number $c\Delta t/h$ is not greater than one.

In this spherically symmetric case we reduce the Kirchhoff integral in (6) to a one-dimensional integral over the angular interval $[0, \pi]$. We choose the trapezoidal rule for the numerical integration (17) used in evaluating this integral, with N_{int} equally spaced integration points in $[0, \pi]$. We also choose

$$\frac{\partial v(\rho, t)}{\partial t} \simeq \frac{v(\rho, t + \Delta t) - v(\rho, t - \Delta t)}{2\Delta t}; \qquad \frac{\partial v(\rho, t)}{\partial \nu} \simeq \frac{v(\rho, t) - v(\rho - v(\rho - h, t)}{h}, \tag{26}$$

as the difference approximations (19).

We set $c = 1$ and $R_\Gamma = 0.1$. We take $g(t) = \sin \omega t$ in (2),

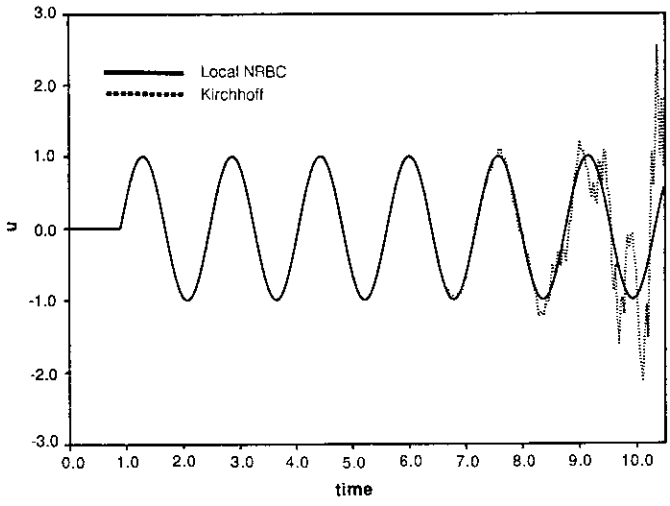

FIG. 3. The solutions $v(R_{\mathcal{B}}, t)$ obtained by using the local NRBC (24) and the Kirchhoff NRBC (6), for $g(t) = \sin 4t$ and the parameters $R_{\mathcal{S}} = 0.7$, $R_{\mathcal{B}} = 1.0$, $N_{gp} = 300$, $N_{int} = 900$, and $\Delta t = 0.0015$.

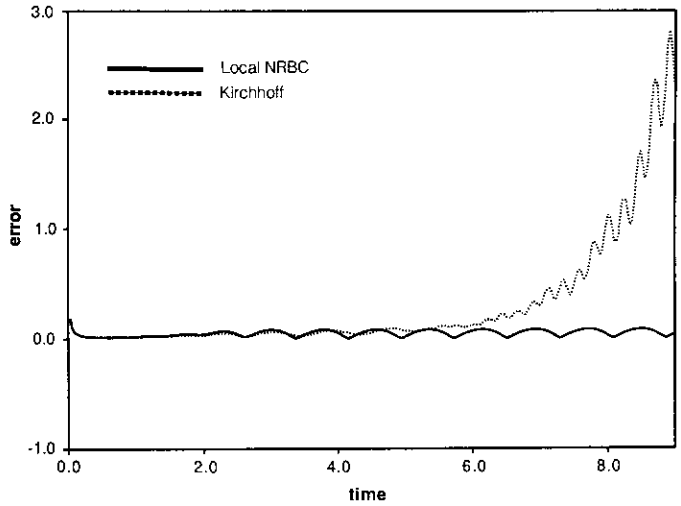

FIG. 4. The normalized errors, as defined by (27), corresponding to the two numerical solutions shown in Fig. 3.

where ω is a given constant frequency. The parameters that are left to be chosen are the frequency ω, $R_{\mathcal{S}}$, $R_{\mathcal{B}}$, the number of grid points N_{gp} (in the radial direction, excluding the point at $\rho = R_\Gamma$), the number of integration points N_{int}, and Δt. The grid parameter h is determined by $h = (R_{\mathcal{B}} - R_\Gamma)/N_{gp}$. The stability condition associated with (25) dictates $\Delta t \leq h/c$. We choose $R_{\mathcal{S}}$ such that $\mathcal{S}$ coincides with a grid point. For each choice of the parameters we obtain a numerical solution by using the Kirchhoff NRBC on $\mathcal{B}$ and another one by using the local NRBC (24) on $\mathcal{B}$. In the latter case, we use the approximations (26) to discretize (24).

First we consider $\omega = 4$, and we choose $R_{\mathcal{S}} = 0.7$, $R_{\mathcal{B}} = 1.0$, $N_{gp} = 300$, and $N_{int} = 900$. Then $h = 0.003$ and we set $\Delta t = h/(2c) = 0.0015$. The two artificial boundaries, $\mathcal{S}$ and $\mathcal{B}$, are 100 grid points apart from each other. Figure 3 shows the two numerical solutions at $\rho = R_{\mathcal{B}}$ as a function of time. Up to about $t = 7$, both solutions agree very well with the exact solution (23), namely they are zero for $t < 0.9$ and behave like the shifted datum g in later times. However, at about $t = 7$ the Kirchhoff solution starts to develop a clear *instability,* which manifests itself by the appearance of rapidly growing oscillations.

We consider the normalized error defined by

$$\text{error}(t) = \|\mathbf{v}_{\text{exact}}(t) - \mathbf{v}_{\text{numerical}}(t)\| / \|\mathbf{v}_{\text{exact}}(t)\|, \qquad (27)$$

where

$$\|\mathbf{v}\| \equiv \left(\sum_A (v_A)^2 \right)^{1/2}. \qquad (28)$$

The sum in (28) is over all the grid points. Figure 4 shows the error corresponding to the two numerical solutions as a function of time. Whereas the error generated by the NRBC (24) remains small, that generated by the Kirchhoff (NRBC) grows exponentially after a certain period of time.

To check the sensitivity of the instability on the type of the boundary data prescribed on the scatterer surface Γ, we replace the persistent wave $g(t) = \sin 4t$ by a short pulse of duration $\pi/4$ with a half sine-wave shape. Figure 5 shows the numerical solutions at $\rho = R_{\mathcal{B}}$ as a function of time. Again, an instability develops in the Kirchhoff case at about $t = 7$, while the solution obtained by using the local NRBC (24) remains stable.

We define $T(e)$ as the smallest value of t which gives, for

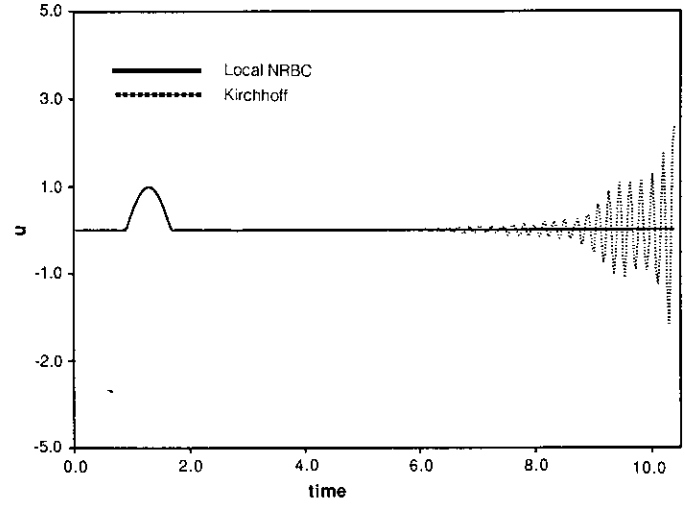

FIG. 5. The solutions $v(R_{\mathcal{B}}, t)$ obtained by using the local NRBC (24) and the Kirchhoff NRBC (6), for $g(t)$ which is a pulse of duration $\pi/4$ with a half sine-wave shape. The same parameters as in Fig. 3 are used.

TABLE I

Various Parameters and the Corresponding Time-to-Instability Measure $T(0.2)$ Obtained by Using the Kirchhoff NRBC on $\mathcal{B}$.

Case	ω	$R_{\mathcal{S}}$	$R_{\mathcal{B}}$	N_{dis}	N_{gp}	N_{int}	h	Δt	$T(0.2)$
1	4	0.8	1.1	3	10	30	0.1	0.05	12.55
2	1								19.05
	0.1								29.10
3								0.09	1.71
								0.01	13.44
4						50			7.25
						100			8.55
5				15	50	150	0.02	0.01	10.25
				30	100	300	0.01	0.005	10.92
6		0.2		9					1.25
		0.6		5					10.45
		1.0		1					2.25
7		1.8	2.1		20	60			20.75
		3.8	4.1		40	120			11.50
8			2.1	13	20	60			5.15
			4.1	33	40	120			7.45
9	4	4.17	4.5	3	40	120	0.11	0.01	101.64

Note. A blank entry indicates the same value as in Case 1.

the Kirchhoff solution, error$(t) \geq e$, using the definition (27). In other words, $T(e)$ is the time it takes the Kirchhoff solution to reach an error of magnitude e. In the case just considered we measured $T(0.2) = 8.57$. We have repeated the numerical solution procedure using the Kirchhoff NRBC with various combinations of parameters and obtained $T(0.2)$ in each case. The value $T(0.2)$ serves as a measure for the time it takes the instability to develop. The instability occurred in all the experiments that we have conducted using the Kirchhoff NRBC incorporated in the nondissipative scheme, although $T(0.2)$ depends strongly on the chosen parameters, as we shall see.

Table I summarizes the result of these experiments. The datum $g = \sin \omega t$ was used in all the experiments. The column N_{dis} indicates the distance in number of grid points between $\mathcal{S}$ and $\mathcal{B}$. The first line of data, denoted "Case 1," is the basic configuration that we refer to in later experiments. A blank entry in Table I means that the corresponding value is the same as in Case 1. For the parameters of Case 1 we obtain $T(0.2) = 12.55$. This result is better than the one obtained in the case considered previously; not only the instability develops later, but also the computational effort in Case 1 is much smaller due to the crudeness of the discretization in space and time. This shows that a careful choice of the parameters may lead to significant improvements.

The following conclusions may be drawn from the results presented in Table I (and from other experimental results which are not presented) with regard to the influence of the various parameters on the time it takes the solution to exhibit an instability:

1. The solution remains stable longer for lower frequencies.

2. Longer times to instability are obtained with smaller time steps.

3. The ratio $N_{\text{int}}/N_{\text{gp}} = 3$ yields the best results as far as the time to instability is concerned.

4. There is an optimal value for the distance between $\mathcal{S}$ and $\mathcal{B}$, for which the time to instability is minimized. In our case it is the value $R_{\mathcal{S}} = 0.8$, which corresponds to a distance of $N_{\text{dis}} = 3$ grid points between $\mathcal{S}$ and $\mathcal{B}$.

In the last case described in Table 1 (Case 9) we fixed $N_{\text{gp}} = 40$ and $\Delta t = 0.01$, which amounts to a fixed computational effort, and we looked for the configuration that would give the longest time to instability. The parameters $R_{\mathcal{S}} = 4.17$, $R_{\mathcal{B}} = 4.5$, and $N_{\text{int}} = 120$ yield $T(0.2) = 101.64$, which was the best result we obtained. The same parameters but with $\omega = 0.1$ give $T(0.2) = 158.90$.

We have also implemented the scheme for the general *asymmetric* three-dimensional case and applied it to a few model problems. We used a spherical artifical boundary as before, but with asymmetric initial data. Accurate results have been obtained up to a certain point in time, when numerical instability started to develop as in the spherically symmetric case. This is of course expected, since the symmetric unstable mode exists in the asymmetric case as well.

A ONE-DIMENSIONAL MODEL PROBLEM

The instability observed in the numerical experiments above is hard to analyze, even in the context of spherically symmetric waves, due to the complexity involved in treating the integral in the right side of the Kirchhoff NRBC (6), or its discretization

(20). Therefore, we consider here a simplified model problem which is easier to handle and gives more insight into the instability phenomenon.

We consider *one-dimensional waves* propagating in a semi-infinite rod or plane waves in the semi-infinite space $x > 0$. The governing equations for the wave $u(x, t)$ are

$$\frac{\partial^2 u}{\partial t^2} = c^2 \frac{\partial^2 u}{\partial x^2}, \quad x > 0, \tag{29}$$

$$u(0, t) = g(t), \tag{30}$$

$$u(x, 0) = \frac{\partial u}{\partial t}(x, 0) = 0, \quad x > 0. \tag{31}$$

The exact solution of (29)–(31) is $u = g(t - x/c)$ if $t \geq x/c$, and $u = 0$ otherwise. Analogously to the three-dimensional case, we introduce the two artificial boundaries $x = X_{\mathcal{G}}$ and $x = X_{\mathcal{B}}$. An exact local NRBC on $\mathcal{B}$ in this simple case is the well-known Sommerfeld condition [1],

$$c \frac{\partial u}{\partial x} + \frac{\partial u}{\partial t} = 0, \quad x = X_{\mathcal{B}}. \tag{32}$$

Note that this NRBC has the same form as the NRBC (24), although (24) involves the variable $v = \rho u$ rather than u itself.

Now we construct a NRBC which is the one-dimensional analogue of the Kirchhoff NRBC (6). It is

$$u(X_{\mathcal{B}}, t) = u(X_{\mathcal{G}}, t - (X_{\mathcal{B}} - X_{\mathcal{G}})/c). \tag{33}$$

This condition simply states that information propagates to the right with speed c; thus the value of u at $X_{\mathcal{B}}$ at time t is the same value at $X_{\mathcal{G}}$ at the retarded time $\tau = t - d/c$, where d is the distance $X_{\mathcal{B}} - X_{\mathcal{G}}$. Clearly the NRBC (33) is exact. It has the same properties as the Kirchhoff NRBC (6), namely it involves the history at $x = X_{\mathcal{G}}$ and yet only a fixed amount of this history. On the other hand, the NRBC (33) is much easier to analyze than (6). We choose the ratio $\Delta t/h$ such that $hN_{\text{dis}}/c = N_{\text{step}}\Delta t$, where N_{step} is an integer number. Then the discrete version of (33) is $u_{\text{gp}}^{n+1} = u_{N_{\text{gp}}-N_{\text{dis}}}^{n+1-N_{\text{step}}}$.

One important difference between (6) and (33) is that (6) involves an integration, which we perform numerically (see (17)), and (33) does not. It may seem possible that the instability previously observed in the three-dimensional case is generated by inaccuracies associated with the calculation of the Kirchhoff integral, and hence it would not appear in the one-dimensional case. To check this, we have implemented a scheme to solve (29)–(31) and (33), using the nondissipative central difference stencil (25) (where v is replaced by u). We set $c = 1$, $g = \sin t$, $X_{\mathcal{B}} = 1.0$, $N_{\text{gp}} = 10$, and $\Delta t = 0.05$. The two artificial boundaries are N_{dis} grid points apart, where N_{dis} is an integer between 1 and 9.

The result of this experiment was that instability appeared

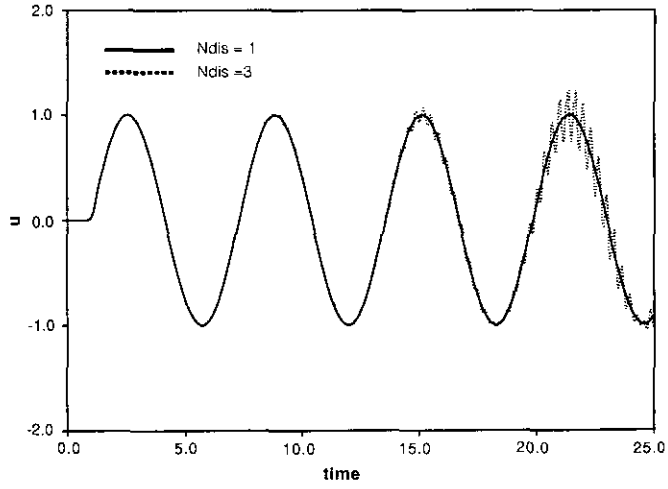

FIG. 6. Solutions $u(X_{\mathcal{B}}, t)$ of the one-dimensional model problem obtained by using the Kirchhoff-type NRBC, for $N_{\text{dis}} = 1$ and $N_{\text{dis}} = 3$.

for all values of N_{dis} *except the value* $N_{\text{dis}} = 1$. Figure 6 shows the numerical solution obtained at $x = X_{\mathcal{B}}$ with $N_{\text{dis}} = 1$ and $N_{\text{dis}} = 3$. The instability which develops in the latter case at about $t = 8$ is clear. This demonstrates that the instability generated by the Kirchhoff NRBC (6) is not related to the calculation of the integral which appears in that formula, but it is associated with the "retarded-time property" which is inherent in (33) as well.

We analyze this instability in a simple special case. We consider the problem (29)–(31) and (33), and discretize it using *three* grid points (plus the one at the boundary $x = 0$). Thus $X_{\mathcal{B}} = 3h$. We also choose $\Delta t = h/(2c)$. The discrete equations are

$$u_0^{n+1} = g(t_{n+1}) \tag{34}$$

$$u_1^{n+1} = 0.25\, u_0^n + 1.5\, u_1^n + 0.25\, u_2^n - u_1^{n-1} \tag{35}$$

$$u_2^{n+1} = 0.25\, u_1^n + 1.5\, u_2^n + 0.25\, u_3^n - u_2^{n-1} \tag{36}$$

$$u_3^{n+1} = \begin{cases} u_2^{n-1}, & N_{\text{dis}} = 1, \\ u_1^{n-3}, & N_{\text{dis}} = 2. \end{cases} \tag{37}$$

Equation (34) is the discrete version of (30). Equations (35) and (36) are obtained from the central difference stencil (25), which is stable for our choice of Courant number, $c\Delta t/h = 1/2$. Equation (37) is the discrete version of the NRBC (33).

To check the stability of the scheme (34)–(37), we first bring it to the matrix form $\mathbf{U}^{n+1} = \mathbf{D}\mathbf{U}^n$. Let $\mathbf{u}^n$ be the three-dimensional vector whose entries are u_1^n, u_2^n, and u_3^n. Then (34)–(37) may be written as

$$\mathbf{u}^{n+1} = \mathbf{A}\mathbf{u}^n + \mathbf{B}\mathbf{u}^{n-1} + \mathbf{C}\mathbf{u}^{n-3} + \mathbf{F}^n, \tag{38}$$

where

$$\mathbf{A} = \begin{bmatrix} 1.5 & 0.25 & 0 \\ 0.25 & 1.5 & 0.25 \\ 0 & 0 & 0 \end{bmatrix}, \quad \mathbf{B} = \begin{bmatrix} -1 & 0 & 0 \\ 0 & -1 & 0 \\ 0 & I_1 & 0 \end{bmatrix},$$

$$\mathbf{C} = \begin{bmatrix} 0 & 0 & 0 \\ 0 & 0 & 0 \\ I_2 & 0 & 0 \end{bmatrix}. \tag{39}$$

$$\mathbf{F}^n = \{0.25 g(t_n)\ 0\ 0\}. \tag{40}$$

In (39) $I_1 = 1$, $I_2 = 0$ if $N_{\text{dis}} = 1$, and $I_1 = 0$, $I_2 = 1$ if $N_{\text{dis}} = 2$. Now we define the three auxiliary variables,

$$\mathbf{P}^n = \mathbf{u}^{n-1}; \quad \mathbf{q}^n = \mathbf{u}^{n-2}; \quad \mathbf{r}^n = \mathbf{u}^{n-3}. \tag{41}$$

Then (38) and (41) can be written in the augmented form,

$$\begin{Bmatrix} \mathbf{u} \\ \mathbf{p} \\ \mathbf{q} \\ \mathbf{r} \end{Bmatrix}^{n+1} = \begin{bmatrix} \mathbf{A} & \mathbf{B} & \mathbf{0} & \mathbf{C} \\ \mathbf{I} & \mathbf{0} & \mathbf{0} & \mathbf{0} \\ \mathbf{0} & \mathbf{I} & \mathbf{0} & \mathbf{0} \\ \mathbf{0} & \mathbf{0} & \mathbf{I} & \mathbf{0} \end{bmatrix} \begin{Bmatrix} \mathbf{u} \\ \mathbf{p} \\ \mathbf{q} \\ \mathbf{r} \end{Bmatrix}^{n} + \begin{Bmatrix} \mathbf{F}^n \\ \mathbf{0} \\ \mathbf{0} \\ \mathbf{0} \end{Bmatrix}. \tag{42}$$

This is a 12-dimensional system of equations. The submatrices **I** are the three-dimensional unit matrices. We denote the augmented matrix in (42) by **D**. To examine the stability of the scheme we consider the homogeneous version of (42), namely we set $g \equiv 0$ in (40). Then (42) assumes the desired form $\mathbf{U}^{n+1} = \mathbf{D}\mathbf{U}^n$.

Now, the stability of the scheme is determined from the *spectral radius* of the matrix **D**, denoted $\rho(\mathbf{D})$. The scheme is unstable if $\rho(\mathbf{D}) \equiv \max|\lambda_i(\mathbf{D})| > 1$, where the $\lambda_i(\mathbf{D})$ are the eigenvalues of **D**. We applied an eigenvalue-finder software to the matrix in (42) and obtained $\rho(\mathbf{D}) = 0.892$ for the case $N_{\text{dis}} = 1$ and $\rho(\mathbf{D}) = 1.016$ for the case $N_{\text{dis}} = 2$.

These results agree with our earlier observation that the scheme is stable for $N_{\text{dis}} = 1$, but unstable for $N_{\text{dis}} \geq 2$. The fact that $\rho(\mathbf{D})$ is only *slightly* larger than one in the unstable case explains the relatively long time that it takes for the instability to manifest itself in the numerical solution. In fact, it can be shown that the measure for the time to instability $T(e)$ that we have considered before, is of order $1/\log \rho(\mathbf{D})$. Thus, if $\rho(\mathbf{D})$ is almost 1 then $T(e)$ is large.

It seems that the three-dimensional case is very similar in character. In fact, the time-to-instability results obtained in the one- and three-dimensional cases were found experimentally to be quite similar. The spectral radius of the amplification matrix is apparently slightly larger than one (although this is hard to check directly), and it can be made closer to one by a careful choice of the computational parameters, as our experiments in the previous section show. We note that in the three-dimensional case we did not obtain a stable solution for any choice of N_{dis} (see Table I), unlike the one-dimensional case, where $N_{\text{dis}} = 1$ leads to a stable scheme.

A DISSIPATIVE NUMERICAL SCHEME

Now we replace the non-dissipative interior stencil (25) by a dissipative stencil. We choose the Lax–Wendroff scheme, which is explicit, dissipative, second-order accurate in space and time, and stable if $c\Delta t/h \leq 1$ [19]. First we apply it to the one-dimensional model problem (29)–(31). In order to do this, we recast the wave equation (29) as a system of two first-order equations. We define $Y_1 = \partial u/\partial t$ and $Y_2 = c\,\partial u/\partial x$. Then (29) is written as

$$\frac{\partial \mathbf{Y}}{\partial t} + \mathbf{E}\frac{\partial \mathbf{Y}}{\partial x} = 0, \tag{43}$$

where

$$\mathbf{Y} = \begin{Bmatrix} Y_1 \\ Y_2 \end{Bmatrix}, \quad \mathbf{E} = \begin{bmatrix} 0 & -c \\ -c & 0 \end{bmatrix}. \tag{44}$$

Now the Lax–Wendroff scheme for (43) is

$$\begin{aligned} Y_A^{n+1} = Y_A^n - \frac{\Delta t}{2h}\mathbf{E}\,(Y_{A+1}^n - Y_{A-1}^n) \\ + \frac{1}{2}\left(\frac{\Delta t}{h}\right)^2 \mathbf{E}^2\,(Y_{A+1}^n - 2Y_A^n + Y_{A-1}^n). \end{aligned} \tag{45}$$

Note that from (44) $\mathbf{E}^2 = c^2\,\mathbf{I}$, and so $\mathbf{E}^2$ in (45) may be replaced by the scalar c^2. The explicit formula (45) is used to update all the interior grid points.

We must accompany (45) by boundary and initial conditions. It is easy to see that the Kirchhoff-type NRBC (33) maintains its form when written in terms of the vector **Y**; namely it becomes

$$\mathbf{Y}(X_{\mathcal{B}}, t) = \mathbf{Y}(X_{\mathcal{G}}, t - (X_{\mathcal{B}} - X_{\mathcal{G}})/c). \tag{46}$$

In other words, not only u, but also the derivatives Y_1 and Y_2 "propagate to the right" with speed c. Similarly, the discrete version of (46) is $\mathbf{Y}_{N_{\text{gp}}}^{n+1} = \mathbf{Y}_{N_{\text{gp}}-N_{\text{dis}}}^{n+1-N_{\text{step}}}$. The boundary condition (30) at $x = 0$ implies $(Y_1)_0^{n+1} = \dot{g}^{n+1}$, where $\dot{g}^{n+1}$ is the value of the derivative of $g(t)$ at time step $n+1$. A boundary condition for Y_2 at $x = 0$ is also needed. Applying forward difference approximation in x and t to the second equation in (43), we obtain

$$(Y_2)_0^{n+1} = (Y_2)_0^n + \frac{\Delta t}{h}((Y_1)_1^n - (Y_1)_0^n). \tag{47}$$

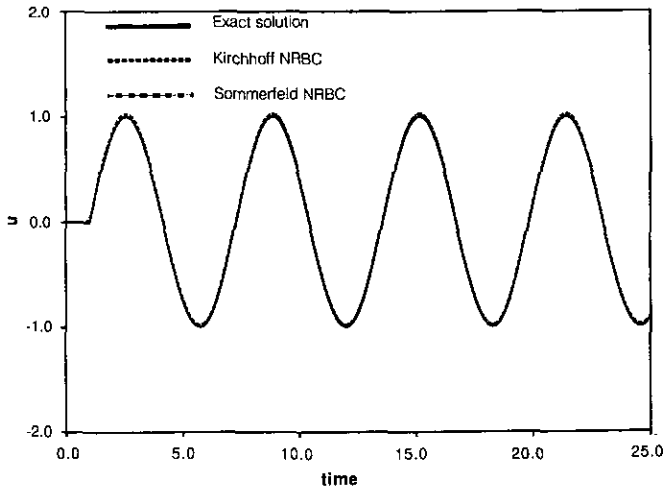

FIG. 7. Solutions $u(X_{\mathcal{B}}, t)$ of the one-dimensional model problem obtained by using a dissipative scheme.

From (31) we deduce the initial condition $\mathbf{Y}_A^0 = 0$, for all grid points A.

We also write the Sommerfeld NRBC (32) in terms of $\mathbf{Y}$. From (32) we have $Y_1 + Y_2 = 0$ at $x = X_{\mathcal{B}}$. We differentiate this equation in time and use the second equation in (43) to get $\partial Y_1/\partial t + c\,\partial Y_1/\partial x = 0$. Then we apply the difference approximations (26). In this way we get the two boundary conditions.

$$(Y_1)_{N_{gp}}^{n+1} = (Y_1)_{N_{gp}}^{n} - \frac{\Delta t}{h}((Y_1)_{N_{gp}}^{n} - (Y_1)_{N_{gp}-1}^{n}),$$
$$(Y_2)_{N_{gp}}^{n+1} = -(Y_1)_{N_{gp}}^{n+1}. \tag{48}$$

We use the Lax–Wendroff interior stencil (45) and either the Kirchhoff or the Sommerfeld NRBC at $x = X_{\mathcal{B}}$. In each time step we obtain the approximate values of Y_1 and Y_2. In order to obtain an approximation to the original variable u itself, we integrate $Y_1 \equiv \partial u/\partial t$ in time by using after time step $n + 1$ the centered formula

$$u_A^{n+1} = u_A^n + \frac{\Delta t}{2}((Y_1)_A^{n+1} + (Y_1)_A^n). \tag{49}$$

We set $c = 1$, $g = \sin t$, $X_{\mathcal{B}} = 1.0$, $N_{gp} = 10$, $\Delta t = 0.05$, and $N_{dis} = 3$. These are exactly the same parameters which were used previously to obtain the results shown in Fig. 6 in the nondissipative case. The solution u at $x = X_{\mathcal{B}}$ as a function of time is shown in Fig. 7. The graphs corresponding to the exact solution and to the solutions obtained by using the Kirchhoff and Sommerfeld NRBCs are compared. We see that no instability arises in the Kirchhoff solution and, moreover, it is slightly more accurate than the Sommerfeld solution. No instability was exhibited with any other choice of the parameters as well.

Now we turn to the three-dimensional case. We apply the dissipative scheme to the spherically symmetric problem described previously (see (22), (23)). We set $c = 1$, $R_\Gamma = 0.1$, $g = \sin 4t$, $R_{\mathcal{S}} = 0.7$, $R_{\mathcal{B}} = 1.0$, $N_{gp} = 300$, $N_{int} = 900$, and $\Delta t = 0.0015$. These are exactly the same parameters which were used to obtain Figs. 3 and 4 in the nondissipative case. In Fig. 8 we show the normalized global errors, as defined by (27), corresponding to the numerical solutions obtained by using the local NRBC (24) and the Kirchhoff NRBC. Thus, the errors shown in Fig. 4 for the nondissipative case may be compared to those shown in Fig. 8 for the dissipative case. Again, we see that no instability is generated in the latter.

The relative errors corresponding to the local and Kirchhoff NRBCs are very similar, and cannot be distinguished in Fig. 8. Note the relatively large errors for very small times. They are the result of using the derivatives of u with respect to x and t as the primal variables in (43), rather than u itself. There is an incompatibility when $t \to 0$ between the boundary condition $Y_1(R_\Gamma, t) = 4 \cos 4t$ for $t > 0$ and the initial condition $Y_1(\rho, 0) = 0$. Thus, *the solution Y_1 is discontinuous in time at $t = 0$*, and the Lax–Wendroff scheme spuriously "smears" this discontinuity.

STABILITY ANALYSIS FOR THE DISSIPATIVE CASE

In this section we consider the one-dimensional model problem (29)–(31) and prove that the scheme consisting of the dissipative Lax–Wendroff interior stencil (45) and the Kirchhoff NRBC (46) on the artificial boundary is indeed stable. We use the Goldberg–Tadmor general theory [20, 21] to establish stability. As opposed to the well-known GKS theory [22], the Goldberg–Tadmor theory provides only sufficient criteria for stability. However, it is much simpler to apply in practice than the GKS theory, and so in many cases it provides a convenient

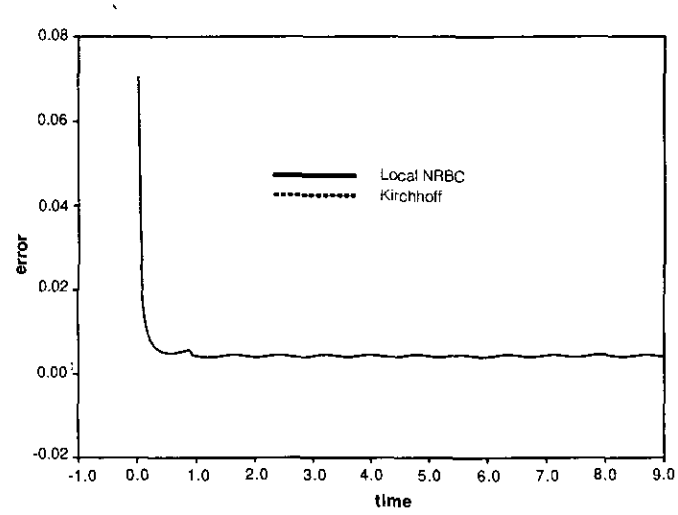

FIG. 8. The normalized errors, as defined by (27), generated by the dissipative scheme using the local NRBC (24) and the Kirchhoff NRBC (6).

alternative to the latter. In both theories, stability is examined in the sense of Definition 3.3 in [22], namely in the sense of uniform boundedness of the solution in finite time intervals.

The first step needed in order to apply the Goldberg–Tadmor theory is to diagonalize the system (43). This is easily done, and we reduce (43) to the two uncoupled equations,

$$\frac{\partial y_1}{\partial t} + c\frac{\partial y_1}{\partial x} = 0, \quad \frac{\partial y_2}{\partial t} - c\frac{\partial y_2}{\partial x} = 0. \tag{50}$$

The first equation corresponds to outgoing waves (with reference to the right boundary $x = X_{\mathcal{B}}$), whereas the second corresponds to incoming waves. According to [20] only the first equation is to be tested for stability. It is also easy to show that the Kirchhoff boundary condition applies to the uncoupled variables y_1 and y_2. Thus,

$$y_1(X_{\mathcal{B}}, t) = y_1(X_{\mathcal{S}}, t - (X_{\mathcal{B}} - X_{\mathcal{S}})/c). \tag{51}$$

The left boundary condition at $x = 0$ is ignored in the stability analysis. This is permitted since if the left and right semi-infinite problems are stable, then by Theorem 5.4 of [22] the two-boundary problem is also stable.

Now we refer to Theorems 2.1 and 2.2 in [20]. They provide several criteria for the stability of the scheme. One of these criteria states that the scheme is stable if (a) the interior stencil is dissipative, (b) the interior stencil is two-level, and (c) the boundary condition satisfies the von Neumann condition and is boundedly solvable. Conditions (a) and (b) are satisfied by the Lax–Wendroff scheme (45). The Kirchhoff boundary condition (51) is explicit; hence it is boundedly solvable by Lemma 2.1 of [20]. Thus it remains to show that (51) satisfies the von Neumann condition, which is defined in [20] in terms of the "boundary characteristic function."

The boundary characteristic function is defined as

$$R(z, \kappa) = \sum_{j=0}^{m} C_j(z)\,\kappa^j, \tag{52}$$

where

$$C_j(z) = C_{j(-1)} - \sum_{\sigma=0}^{q} z^{-\sigma-1}\, C_{j\sigma}. \tag{53}$$

Here, m, q, and the coefficients $C_{j\sigma}$ are parameters of the boundary condition under consideration. In the case of the Kirchhoff boundary condition (51), the only nonzero coefficients are $C_{0(-1)} = 1$ and $C_{(N_{\text{dis}})(N_{\text{step}}-1)} = 1$. From (53), $C_j(z) = \delta_{j0} - z^{-N_{\text{step}}}\,\delta_{j(N_{\text{dis}})}$, where $\delta_{j\sigma}$ is the Kronecker delta. Thus the boundary characteristic function for the Kirchhoff condition is

$$R(z, \kappa) = 1 - z^{-N_{\text{step}}}\,\kappa^{N_{\text{dis}}}. \tag{54}$$

We remark that the functions $C_j(z)$ in our case satisfy Assumption 1.5 in [20] which is essential for stability.

Now, according to Definition 2.2 in [20], the boundary condition satisfies the von Neumann condition if the roots $z(\kappa)$ of $R(z, \kappa) = 0$ satisfy $|z(\kappa)| \leq 1$ for all $|\kappa| = 1$. In our case, (54) gives the roots $z(\kappa) = \kappa^{N_{\text{dis}}/N_{\text{step}}}$, which obviously satisfy the condition. Thus, stability is established.

CONCLUDING REMARKS

We have considered numerical schemes which involve nonlocal Kirchhoff-type NRBCs. These NRBCs are *exact*, and hence they ensure highly accurate numerical results, if discretized properly. Moreover, they do not entail large computational effort and avoid the difficulties otherwise encountered in the application of exact NRBCs in the time-dependent case. Therefore, the use of Kirchhoff-type NRBCs for three-dimensional time-dependent problems of acoustic and elastic waves holds a lot of promise.

We observed that a long-time instability develops if the interior stencil used is nondissipative. However, it is possible to delay the time to instability by careful parametrization. Moreover, it is possible to totally eliminate the instability by using a *dissipative* interior stencil.

Phenomena of weak instabilities generated by boundary conditions in hyperbolic initial boundary value problems were discussed by Trefethen [23]. His theory, which extends the GKS theory [22], shows that such instabilities are caused by spurious radiation of wave energy from the boundary at a nonnegative numerical group velocity. Numerical demonstration of these effects in the context of nonreflecting boundary conditions is given in [24].

A numerical procedure which is different than the one considered here, but related to it, was proposed in [1]. In this procedure, one takes the normal derivative of the Kirchhoff formula (6) and then considers the limit when $\mathcal{S}$ approaches $\mathcal{B}$. This results in an exact nonlocal NRBC which involves a single artificial boundary and preserves the good qualities of the Kirchhoff NRBC. However, the stability properties of this new NRBC are unknown and must be investigated.

ACKNOWLEDGMENTS

This work was partly supported by the L. Kraus Research Fund, VPRF No. 160–700, and by the Fund for the Promotion of Research at the Technion. The authors are grateful to Reviewer 2 for his/her very helpful remarks, and to Prof. M. Goldberg for his assistance.

REFERENCES

1. D. Givoli, *Numerical Methods for Problems in Infinite Domains* (Elsevier, Amsterdam, 1992).
2. D. Givoli, *J. Comput. Phys.* **94,** 1 (1991).
3. B. Engquist and A. Majda, *Math. Comput.* **31,** 629 (1977).

4. A. Bayliss and E. Turkel, *Commun. Pure Appl. Math.* **33,** 707 (1980).
5. T. Hagstrom and H. B. Keller, *SIAM J. Math. Anal.* **17,** 322 (1986).
6. J. B. Keller and D. Givoli, *J. Comput. Phys.* **82,** 172 (1989).
7. D. Givoli and J. B. Keller, *Comput. Methods Appl. Mech. Eng.* **76,** 41 (1989).
8. D. Givoli and J. B. Keller, *Wave Motion,* **12,** 261 (1990).
9. E. A. Trautenberg, K. Gebauer, and A. Sachs, "Numerical Simulation of Wave Propagation in Viscoelastic Media with Non-Reflecting Boundary Conditions," *Wave Propagation in Viscoelastic Media,* edited by F. Mainardi (Pitman, London, 1982), p. 194.
10. L. Wagatha, *Appl. Numer. Math.* **1,** 309 (1985).
11. M. Beland and T. Warn, *J. Atmos. Sci.* **32,** 1873 (1975).
12. B. Gustafsson, *SIAM J. Sci. Stat. Comput.* **9,** 812 (1988).
13. D. Givoli, *Comput. Methods Appl. Mech. Eng.* **95,** 97 (1992).
14. L. Ting and M. J. Miksis, *J. Acoust. Soc. Am.* **80,** 1825 (1986).
15. B. B. Baker and E. T. Copson, *The Mathematical Theory of Huygen's Principle* (Oxford Univ. Press, London, 1953).
16. D. S. Jones, *The Theory of Electromagnetism* (Macmillan & Co., London, 1964).
17. L. T. Wheeler and E. Sternberg, *Arch. Rat. Mech. Anal.* **31,** 51 (1968).
18. J. D. Achenbach, *Wave Propagation in Elastic Solids* (North-Holland, Amsterdam, 1973).
19. A. R. Mitchell and D. F. Griffiths, *The Finite Difference Method in Partial Differential Equations* (Wiley, New York, 1980).
20. M. Goldberg and E. Tadmor, *Math. Comput.* **44,** 361 (1985).
21. M. Goldberg and E. Tadmor, *Math. Comput.* **48,** 503 (1987).
22. B. Gustafsson, H.-O. Kreiss, and A. Sundström, *Math. Comput.* **26,** 649 (1972).
23. L. N. Trefethen, *Commun. Pure Appl. Math.* **37,** 329 (1984).
24. R. L. Higdon, *Math. Comput.* **47,** 437 (1986).